J. Mod. Power Syst. Clean Energy (2019) 7(6):1697–1708
https://doi.org/10.1007/s40565-019-0520-y

Analysis of unbalanced clustered voltage and control strategy of clustered voltage balancing for cascaded H-bridge STATCOM

Yu JIN[1], Jianze WANG[1], Yiqi LIU[2], Xinagyu SAI[1], Yanchao JI[1]

Abstract To explore the clustered voltage balancing mechanism of the cascaded H-bridge static synchronous compensator (STATCOM), this paper analyzes the causes of unbalanced clustered voltage. The negative-sequence current caused by the compensation of unbalanced reactive power or detection and control errors and the zero-sequence voltage caused by voltage drift of the STATCOM neutral point contribute to unbalanced clustered voltage. On this basis, this paper proposes a control strategy to inject negative-sequence current and zero-sequence voltage simultaneously. The injection of negative-sequence current may cause current asymmetry in the grid, and the zero-sequence injection has a relatively limited balancing ability in the clustered voltages. The proposed control strategy can not only generate a faster balancing response than the traditional zero-sequence voltage injection method, but also lower the extent of current asymmetry compared with the traditional negative-sequence current injection method. Then, the negative-sequence current and zero-sequence voltage injection are further transformed into the *dq* frame to establish a unified frame. The effectiveness of the proposed control strategy is verified by the simulation and experimental results.

Keywords Cascaded static synchronous compensator (STATCOM), Clustered voltage, Control strategy, Negative-sequence current, Zero-sequence voltage

Croscheck date: 21 December 2018

Received: 28 December 2017 / Accepted: 21 December 2018 / Published online: 19 April 2019

✉ Yanchao JI
hitjyc2016@163.com

Yu JIN
hitjy19940213@163.com

Jianze WANG
jzwang.hit@yahoo.com

Yiqi LIU
liuyq0925@126.com

Xinagyu SAI
sxy950425@163.com

[1] School of Electrical Engineering and Automation, Harbin Institute of Technology, Harbin, China

[2] College of Mechanical and Electrical Engineering, Northeast Forestry University, Harbin, China

1 Introduction

Static synchronous compensator (STATCOM) plays a significant role in controlling power factor, regulating grid voltage, stabilizing a power system, etc. The cascaded H-bridge topology is a common topology for STATCOMs of high voltage and high power due to its simple structure and modularity [1]. Each of the cascaded H-bridge converters is furnished with an isolated and floating DC capacitor deprived of power source or circuit [2]. The cascaded H-bridge STATCOM injects specific reactive current through capacitors in each H-bridge unit. However, the DC voltage imbalance of the capacitors has been a very critical issue, which affects the safety operation of the STATCOM and leads to system collapse [1]. To ensure the safety operation of the device and to realize precise current control, regulating strategies over voltage balancing of the capacitors are necessary. The causes of unbalanced clustered voltage have been analyzed in [3], and this study attributes this phenomenon to the negative-sequence voltage of a grid. However, the negative-

sequence voltage only accounts for a small portion of the grid voltage; therefore, there should also be other causes for this phenomenon.

To solve the problem of unbalanced DC voltage across each floating capacitor, various research works have been carried out and the resultant papers have been published in [1–23]. The hierarchical voltage balancing structure is first proposed to solve the imbalance problem in [4]. The voltage balancing can be divided into three layers, including overall voltage control, clustered voltage balancing control, and individual voltage balancing control. This paper mainly focuses on the second layer, clustered voltage balancing control. For overall voltage control, a proportional-integral (PI) controller in the *dq* frame is usually adopted to regulate the sum of voltages of all the capacitors in three phases [4, 17, 22]. For individual voltage balancing control, multiple research studies have been conducted in [5–12]. The individual phase instantaneous current tracking method is employed in [5] to control the voltage of each DC capacitor. Reference [6] adopts a novel balance control method for individual DC voltage balancing based on the popular carrier phase-shifted sinusoidal pulse-width modulation (PWM) strategy, and this method makes the control strategy simpler and more flexible. References [13–15] have further proposed the individual voltage balancing strategy based on space vector modulation and another method of current injection, the root-mean-square (RMS) of which is zero, as presented in [16].

For a clustered voltage balancing control, the PI controller is first adopted to regulate the DC clustered voltages of the capacitors in [4]. On this basis, the clustered voltage balancing strategy based on the loop-gain shaping controller in the *dq* frame is described in [22]. However, the injection components of these clustered voltage balancing strategies are not analyzed and the injection components may include positive-sequence and other components that may not be necessary for the clustered voltage balancing. This may lower the efficiency and affect the balancing strategy. Therefore, the voltage balancing technique based on negative-sequence current injection [17] and zero-sequence voltage injection [18] is proposed to eliminate the imbalance of the voltage between the clusters. Based on [17], a new clustered voltage balancing control is realized by regulating the negative-sequence modulation reference voltage in the *dq* frame [1]. Considering the merits and demerits of zero-sequence voltage and negative-sequence current injection, one of the two kinds of injection is applied according to the load currents of the grid in [19, 23]. The zero-sequence voltage injection may lower the DC voltage utilization and have a relatively limited ability in the clustered voltage balancing, while the negative-sequence current injection results in significant peak current and even triggers the current asymmetry of the power grid. Thus, voltage balancing strategies to improve the DC voltage utilization by regulating the effectiveness between the zero-sequence voltage and negative-sequence current injection are proposed [20]. On the basis of these studies, reference [21] provided the voltage balancing strategy to manage the peak current and the modulation index simultaneously. However, it should be noted that the possible demerits, current asymmetry of the grid caused by the negative-sequence injection and the limited ability in the clustered voltage balancing of the zero-sequence injection, remain to be solved.

This paper first analyzes the causes of the unbalanced clustered voltage. The negative-sequence current caused by the unbalanced loads and the zero-sequence voltage caused by the voltage drift of the STATCOM neutral point contribute to this unbalanced clustered voltage. On this basis, a novel control strategy to inject the negative-sequence current and zero-sequence voltage simultaneously is proposed. The proposed control strategy can generate a faster balancing response. It also lowers the extent of current asymmetry by reducing the negative-sequence current injection. To establish a unified frame, the negative-sequence and zero-sequence injections are further transformed into the *dq* frame. The effectiveness of the proposed control strategy is verified by simulation and experimental results.

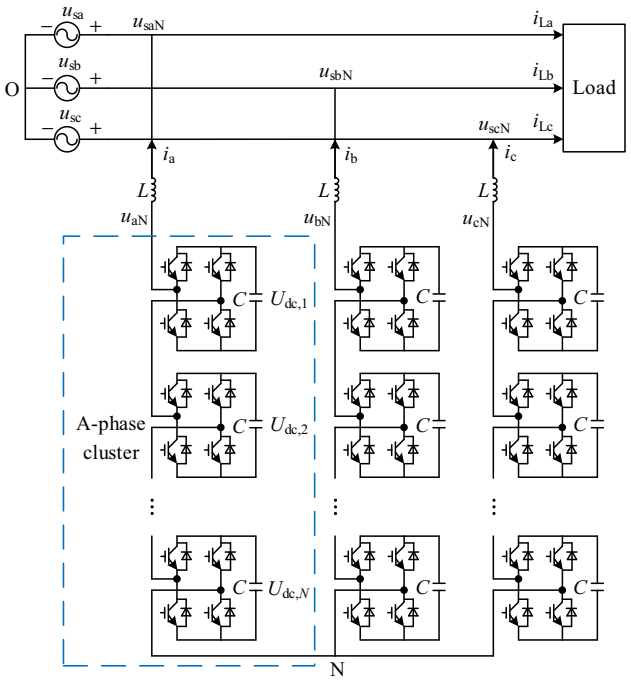

Fig. 1 Circuit configuration of cascaded STATCOM

2 System configuration

The circuit configuration of the cascaded STATCOM is shown in Fig. 1. The cascaded STATCOM is composed of three identical clusters with a star connection. Each cluster consists of N series of H-bridge units and is connected to the grid through an inductance L. u_{sa}, u_{sb}, and u_{sc} are the three-phase grid voltages; u_{aN}, u_{bN}, and u_{cN} are the three-phase output voltages of the STATCOM; i_{La}, i_{Lb}, and i_{Lc} are the three-phase currents of the grid loads; i_a, i_b, and i_c are the three-phase output currents of the STATCOM; $U_{dc,1}$, $U_{dc,2}$, and $U_{dc,N}$ represent the voltages across each capacitor.

3 Analysis of unbalanced clustered voltage

In practical engineering projects, the phenomenon of unbalanced clustered voltages is quite common. Most literatures attribute this phenomenon to the difference of the electronic devices and the unbalanced grid voltage. However, there are other important factors that trigger this problem and few literature studies have been conducted to explore the causes behind this.

Most literatures have not provided any specific instruction on how to measure the output voltage of the cascaded STATCOM and decompose it into only the positive-sequence component [1, 7, 8] and some with minor portions of the negative-sequence component [19–21]. The component of the output voltage is the same as the grid voltage in these circumstances. However, they have not considered the zero-sequence voltage [17, 18]. The voltage of each cluster is a reflection of the active power flow of the STATCOM, and the active power flow of each cluster should be calculated with the output voltage and current of the cascaded STATCOM, i.e., u_{aN}, u_{bN}, u_{cN}, i_a, i_b, and i_c. The active power flow of the converters are replaced with the active power flow of converter together with the inductor in this study because the inductor will absorb no active power from either the grid or the converter. Therefore, the cluster voltages used to calculate the active power flow, u_{aN}, u_{bN}, and u_{cN}, can be replaced by u_{saN}, u_{sbN}, and u_{scN}, as shown in Fig. 1.

The following equations (1)–(3) are derived based on the following assumptions:

1) The grid voltages are balanced and only the positive-sequence voltage exists.
2) The STATCOM generates only the reactive power to correct the power factor, and no additional injection is included to balance the voltage of each capacitor.

Then, the output voltage of each cluster and the current of the cascaded STATCOM can thus be expressed as (1) and (2), respectively.

$$\begin{aligned}\begin{bmatrix} u_{saN} \\ u_{sbN} \\ u_{scN} \end{bmatrix} &= \begin{bmatrix} u_{sa} \\ u_{sb} \\ u_{sc} \end{bmatrix} + \begin{bmatrix} u_{ON} \\ u_{ON} \\ u_{ON} \end{bmatrix} \\ &= U_p \begin{bmatrix} \cos \omega t \\ \cos\left(\omega t - \frac{2}{3}\pi\right) \\ \cos\left(\omega t + \frac{2}{3}\pi\right) \end{bmatrix} + U_0 \begin{bmatrix} \cos(\omega t + \phi_0) \\ \cos(\omega t + \phi_0) \\ \cos(\omega t + \phi_0) \end{bmatrix}\end{aligned} \tag{1}$$

where U_p is the amplitude of the positive-sequence voltage of the grid; ω is the grid frequency; U_0 and ϕ_0 are the amplitude and the phase angle of the zero-sequence voltage, u_{ON}, caused by the voltage drift of the neutral point, respectively.

$$\begin{aligned}\begin{bmatrix} i_a \\ i_b \\ i_c \end{bmatrix} &= I_p \begin{bmatrix} \cos(\omega t + \varphi_p) \\ \cos\left(\omega t + \varphi_p - \frac{2}{3}\pi\right) \\ \cos\left(\omega t + \varphi_p + \frac{2}{3}\pi\right) \end{bmatrix} \\ &\quad + I_n \begin{bmatrix} \cos(\omega t + \varphi_n) \\ \cos\left(\omega t + \varphi_n + \frac{2}{3}\pi\right) \\ \cos\left(\omega t + \varphi_n - \frac{2}{3}\pi\right) \end{bmatrix}\end{aligned} \tag{2}$$

where I_p and φ_p are the amplitude and the phase angle of the positive-sequence output current, respectively; I_n and φ_n are the amplitude and the phase angle of the negative-sequence output current caused by the compensation of unbalanced loads or detection and control errors, respectively.

The active power flow of each cluster can thus be expressed as:

$$\begin{aligned}\begin{bmatrix} P_a \\ P_b \\ P_c \end{bmatrix} &= \frac{1}{T}\int_0^T \begin{bmatrix} u_{saN} i_a \\ u_{sbN} i_b \\ u_{scN} i_c \end{bmatrix} \mathrm{d}t \\ &= \begin{bmatrix} \cos\varphi_p & \cos\varphi_n & \cos(\phi_0 - \varphi_p) & \cos(\phi_0 - \varphi_n) \\ \cos\varphi_p & \cos(\varphi_n - 2\pi/3) & \cos(\phi_0 - \varphi_p + 2\pi/3) & \cos(\phi_0 - \varphi_n - 2\pi/3) \\ \cos\varphi_p & \cos(\varphi_n + 2\pi/3) & \cos(\phi_0 - \varphi_p - 2\pi/3) & \cos(\phi_0 - \varphi_n + 2\pi/3) \end{bmatrix} \begin{bmatrix} U_p I_p \\ U_p I_n \\ U_0 I_p \\ U_0 I_n \end{bmatrix}\end{aligned} \tag{3}$$

where T is the time of each period. It can be seen from (3) that $U_p I_p \cos\varphi_p$ is the same component of P_a, P_b, and P_c that will contribute no imbalance to the three phases. The negative-sequence current caused by the compensation of the unbalanced loads or detection and control errors, and

the zero-sequence voltage caused by the voltage drift of the STATCOM neutral point contribute to the unbalanced voltage of each cluster. This phenomenon is thus inevitable.

4 Control strategy of cascaded STATCOM

Figure 2 illustrates the overall control block diagram of the cascaded STATCOM. The control diagram can be divided into three layers. The first layer, active/reactive power control, is designed to control the overall DC voltage $U_{\mathrm{dc,sum}}$ and correct the grid power factor by generating a reactive power. The second layer, clustered voltage balancing control, aims to balance the three clustered voltages U_{dca}, U_{dcb}, and U_{dcc}. The third layer, an individual voltage balancing control, is to regulate the voltage of each capacitor ($U_{\mathrm{dc}kj}$, k = a, b, c, j = 1, 2, …, N). This paper mainly focuses on the control strategy of the second layer.

4.1 Transformation between different frames

The overall DC voltage control and reactive power control is conducted under the dq frame. However, the traditional clustered voltage balancing control has been calculated in the form of symmetrical components (positive-sequence, negative-sequence, and zero-sequence). In order to keep pace with the dq rotating frame, this paper puts forward a clustered voltage balancing control strategy conducted in the dq frame.

$$\boldsymbol{T}_{pn0}^{dq0}=\boldsymbol{T}_{\alpha\beta0}^{dq0}\boldsymbol{T}_{\mathrm{abc}}^{\alpha\beta0}\boldsymbol{T}_{pn0}^{\mathrm{abc}} \tag{4}$$

$$\boldsymbol{T}_{dq0}^{pn0}=(\boldsymbol{T}_{pn0}^{dq0})^{-1}=(\boldsymbol{T}_{pn0}^{\mathrm{abc}})^{-1}(\boldsymbol{T}_{\mathrm{abc}}^{\alpha\beta0})^{-1}(\boldsymbol{T}_{\alpha\beta0}^{dq0})^{-1} \tag{5}$$

$$\boldsymbol{T}_{\alpha\beta0}^{dq0}=\begin{bmatrix}\sin\omega t & -\cos\omega t & 0\\ -\cos\omega t & -\sin\omega t & 0\\ 0 & 0 & 1\end{bmatrix} \tag{6}$$

$$\boldsymbol{T}_{\mathrm{abc}}^{\alpha\beta0}=\frac{2}{3}\begin{bmatrix}1 & -\frac{1}{2} & -\frac{1}{2}\\ 0 & \frac{\sqrt{3}}{2} & -\frac{\sqrt{3}}{2}\\ \frac{1}{2} & \frac{1}{2} & \frac{1}{2}\end{bmatrix} \tag{7}$$

$$\boldsymbol{T}_{pn0}^{\mathrm{abc}}=\begin{bmatrix}1 & 1 & 1\\ \alpha^2 & \alpha & 1\\ \alpha & \alpha^2 & 1\end{bmatrix} \tag{8}$$

where $\boldsymbol{T}_{pn0}^{dq0}$ is the transformation matrix from sequence frame (positive negative and zero sequence) to dq frame; $\boldsymbol{T}_{dq0}^{pn0}$ is the opposite transformation matrix from dq frame to sequence frame; $\boldsymbol{T}_{pn0}^{\mathrm{abc}}$ is the transformation matrix from sequence frame to abc frame; $\boldsymbol{T}_{\mathrm{abc}}^{\alpha\beta0}$ is the transformation matrix from abc frame to $\alpha\beta$ frame; $\boldsymbol{T}_{\alpha\beta0}^{dq0}$ is the transformation matrix from $\alpha\beta$ frame to dq frame; $\alpha=\mathrm{e}^{\mathrm{j}120^\circ}$.

Equations (4)–(8) are the transformation matrices in this study, (9) and (10) exhibit the transformation between the symmetrical components and the dq frame.

$$\begin{cases}\boldsymbol{u}_{dq0}=\boldsymbol{T}_{pn0}^{dq0}\boldsymbol{u}_{pn0}\\ \boldsymbol{i}_{dq0}=\boldsymbol{T}_{pn0}^{dq0}\boldsymbol{i}_{pn0}\end{cases} \tag{9}$$

$$\begin{cases}\boldsymbol{u}_{pn0}=\boldsymbol{T}_{dq0}^{pn0}\boldsymbol{u}_{dq0}\\ \boldsymbol{i}_{pn0}=\boldsymbol{T}_{dq0}^{pn0}\boldsymbol{i}_{dq0}\end{cases} \tag{10}$$

4.2 Overall DC voltage control and reactive power control

In this study, the d-axis current and q-axis current were injected individually to control the overall DC voltage and reactive power. Figure 3 shows the block diagram of the overall DC voltage control and reactive power control.

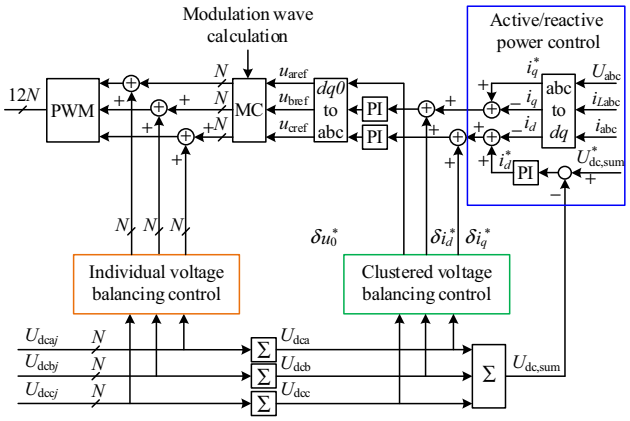

Fig. 2 Overall control block diagram of the cascaded STATCOM

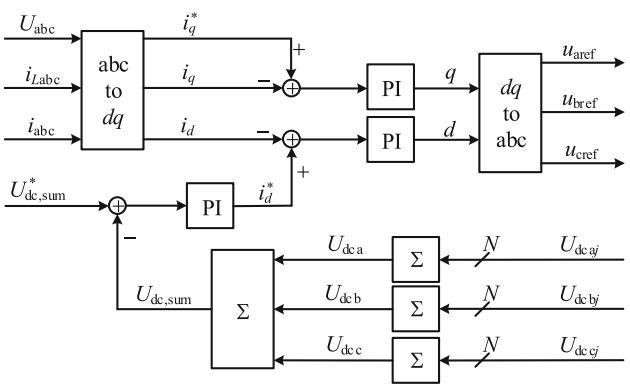

Fig. 3 Block diagram of the overall DC voltage control and reactive power control

Equations (11) and (12) reveal that if the d-axis and q-axis component injections are constant, then they can be transformed into the positive-sequence component exclusively, which will not affect the balance of the clustered voltage. The d-axis current injection is calculated as (13) and the q-axis current injection is calculated as (14).

$$\begin{bmatrix} i_a \\ i_b \\ i_c \end{bmatrix} = \boldsymbol{T}_{dq0}^{abc} \begin{bmatrix} i_d \\ i_q \\ i_0 \end{bmatrix} = (\boldsymbol{T}_{abc}^{\alpha\beta0})^{-1} (\boldsymbol{T}_{\alpha\beta0}^{dq0})^{-1} \begin{bmatrix} i_d \\ i_q \\ i_0 \end{bmatrix} \tag{11}$$

$$\boldsymbol{T}_{dq0}^{abc} = \begin{bmatrix} \sin\omega t & -\cos\omega t & 1 \\ -\frac{1}{2}\sin\omega t - \frac{\sqrt{3}}{2}\cos\omega t & \frac{1}{2}\cos\omega t - \frac{\sqrt{3}}{2}\sin\omega t & 1 \\ -\frac{1}{2}\sin\omega t + \frac{\sqrt{3}}{2}\cos\omega t & \frac{1}{2}\cos\omega t + \frac{\sqrt{3}}{2}\sin\omega t & 1 \end{bmatrix} \tag{12}$$

$$i_d^* = \left(K_{Pov} + \frac{K_{Iov}}{S}\right)\left(U_{dc,sum}^* - U_{dc,sum}\right) \tag{13}$$

$$i_q^* = -Q_{load}/U_d \tag{14}$$

where $\boldsymbol{T}_{dq0}^{abc}$ is the transformation matrix from dq frame to abc frame; K_{Pov} and K_{Iov} are the proportional and integral gains in the PI control loop of the overall DC voltage; Q_{load} is the reactive power generated by the grid loads; U_d is the d-axis component of the output voltages; $U_{dc,sum}^*$ is the reference of overall DC voltage $U_{dc,sum}$.

4.3 Clustered voltage balancing control

Clustered voltage balancing control focuses on regulating the sum voltage of capacitors in each phase cluster and the control target is to keep U_{dca}, U_{dcb} and U_{dcc} equal to the average value.

According to (1) to (3), extra negative-sequence current and zero-sequence voltage injection is necessary since the phenomenon of unbalanced cluster voltage is inevitable. Extra negative-sequence current injection will cause current asymmetry of power grid but has a high efficiency in clustered voltage balancing while extra zero-sequence voltage injection generates no additional influence on current asymmetry but has a relatively low efficiency in clustered voltage balancing. This paper proposes a novel control strategy which injects the negative-sequence current and zero-sequence voltage at the same time. The proposed control strategy can not only generate a stronger balancing ability and a faster balancing response than traditional zero-sequence voltage injection methods, but also lower the extent of current asymmetry compared with traditional negative-sequence current injection methods. The block diagram of the proposed clustered voltage balancing control is shown in Fig. 4. In Fig. 4, δu_0 and δi_n are

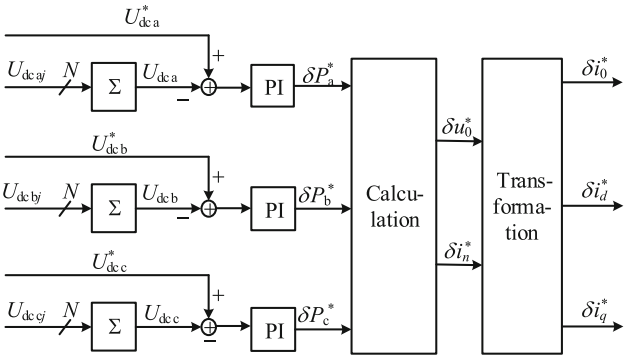

Fig. 4 Block diagram of the proposed clustered voltage balancing control

the zero-sequence voltage and negative-sequence current injected to balance the clustered voltages and they are further transformed into δu_0^*, δi_d^*, and δi_q^*.

1) Overall control strategy: The output voltage, current and active power flow of cascaded STATCOM including no extra injection to balance the voltage of each capacitor are depicted in (1) to (3), and the corresponding voltage, current and additional active power flow of cascaded STATCOM with extra negative-sequence current and zero-sequence voltage injection are illustrated in (15) to (17).

$$\begin{bmatrix} u'_{saN} \\ u'_{sbN} \\ u'_{scN} \end{bmatrix} = U_p \begin{bmatrix} \cos\omega t \\ \cos\left(\omega t - \frac{2}{3}\pi\right) \\ \cos\left(\omega t + \frac{2}{3}\pi\right) \end{bmatrix} + U_0 \begin{bmatrix} \cos(\omega t + \phi_0) \\ \cos(\omega t + \phi_0) \\ \cos(\omega t + \phi_0) \end{bmatrix} + \delta U_0 \begin{bmatrix} \cos(\omega t + \phi'_0) \\ \cos(\omega t + \phi'_0) \\ \cos(\omega t + \phi'_0) \end{bmatrix} \tag{15}$$

$$\begin{bmatrix} i'_a \\ i'_b \\ i'_c \end{bmatrix} = I_p \begin{bmatrix} \cos(\omega t + \varphi_p) \\ \cos\left(\omega t + \varphi_p - \frac{2}{3}\pi\right) \\ \cos\left(\omega t + \varphi_p + \frac{2}{3}\pi\right) \end{bmatrix} + I_n \begin{bmatrix} \cos(\omega t + \varphi_n) \\ \cos\left(\omega t + \varphi_n + \frac{2}{3}\pi\right) \\ \cos\left(\omega t + \varphi_n - \frac{2}{3}\pi\right) \end{bmatrix} + \delta I_n \begin{bmatrix} \cos(\omega t + \varphi'_n) \\ \cos\left(\omega t + \varphi'_n + \frac{2}{3}\pi\right) \\ \cos\left(\omega t + \varphi'_n - \frac{2}{3}\pi\right) \end{bmatrix} \tag{16}$$

$$\begin{bmatrix}\delta P_{\mathrm{a}}\\ \delta P_{\mathrm{b}}\\ \delta P_{\mathrm{c}}\end{bmatrix}=\begin{bmatrix}\cos\varphi_n' & \cos(\phi_0-\varphi_n') & \cos(\phi_0'-\varphi_p) & \cos(\phi_0'-\varphi_n)\\ \cos(\varphi_n'-2\pi/3) & \cos(\phi_0-\varphi_n'-2\pi/3) & \cos(\phi_0'-\varphi_p+2\pi/3) & \cos(\phi_0'-\varphi_n-2\pi/3)\\ \cos(\varphi_n'+2\pi/3) & \cos(\phi_0-\varphi_n'+2\pi/3) & \cos(\phi_0'-\varphi_p-2\pi/3) & \cos(\phi_0'-\varphi_n+2\pi/3)\end{bmatrix}\begin{bmatrix}U_p\delta I_n\\ U_0\delta I_n\\ \delta U_0 I_p\\ \delta U_0 I_n\end{bmatrix} \tag{17}$$

where δU_0 and ϕ_0' are the amplitude and phase angle of δu_0; δI_n and φ_n' are the amplitude and phase angle of δi_n. The higher order minima of power flow, $\delta u_0 \delta i_n$, is omitted in (17). However, there are four variables (δU_0, δI_n, ϕ_0' and φ_n') in two linear independent equations according to the referential power flow of each phase cluster, as δP_{a} $+ \delta P_{\mathrm{b}} + \delta P_{\mathrm{c}} = 0$. So, this paper will add additional restrictive conditions to make the maximum utilization of the two kinds of injection. These restrictive conditions will help to calculate two of the variables, ϕ_0' and φ_n', respectively. Then, the four variables will be calculated according to the two-linear independent equation in (17), thus deriving the negative-sequence current and zero-sequence voltage injection components.

2) Calculation of phase angle: The phase angles of zero-sequence voltage injection and negative-sequence current injection are calculated according to the following principles.

The selection principles of phase angle for injection of zero-sequence voltage are discussed first. In order to make maximum utilization of the zero-sequence voltage injection, the phase angle ϕ_0' can be calculated using two alternative principles. The first principle is to provide the maximum active power flow with the same amplitude of δU_0, and the phase angle ϕ_0' is calculated using (18)–(20).

If $\max\{|\delta P_{\mathrm{a}}^*|, |\delta P_{\mathrm{b}}^*|, |\delta P_{\mathrm{c}}^*|\} = |\delta P_{\mathrm{a}}^*|$, then

$$\phi_0' = \begin{cases}\varphi_p & \delta P_{\mathrm{a}}^* \geq 0\\ \varphi_p + \pi & \delta P_{\mathrm{a}}^* < 0\end{cases} \tag{18}$$

If $\max\{|\delta P_{\mathrm{a}}^*|, |\delta P_{\mathrm{b}}^*|, |\delta P_{\mathrm{c}}^*|\} = |\delta P_{\mathrm{b}}^*|$, then

$$\phi_0' = \begin{cases}\varphi_p - 2\pi/3 & \delta P_{\mathrm{b}}^* \geq 0\\ \varphi_p + \pi/3 & \delta P_{\mathrm{b}}^* < 0\end{cases} \tag{19}$$

If $\max\{|\delta P_{\mathrm{a}}^*|, |\delta P_{\mathrm{b}}^*|, |\delta P_{\mathrm{c}}^*|\} = |\delta P_{\mathrm{c}}^*|$, then

$$\phi_0' = \begin{cases}\varphi_p + 2\pi/3\delta & P_{\mathrm{c}}^* \geq 0\\ \varphi_p - \pi/3 & \delta P_{\mathrm{c}}^* < 0\end{cases} \tag{20}$$

The second principle is to alter the least amplitude of overall voltage in each phase cluster with the same amplitude of δU_0, and the phase angle ϕ_0' is calculated using (21)–(23).

Both the principles are effective. However, the first principle can generate more significant effect on the active power flow. This paper adopts the first principle to calculate the phase angle of zero-sequence voltage injection.

If $\max\{|\delta P_{\mathrm{a}}^*|, |\delta P_{\mathrm{b}}^*|, |\delta P_{\mathrm{c}}^*|\} = |\delta P_{\mathrm{a}}^*|$, then

$$\phi_0' = \begin{cases}0 & \delta P_{\mathrm{a}}^* \geq 0\\ \pi & \delta P_{\mathrm{a}}^* < 0\end{cases} \tag{21}$$

If $\max\{|\delta P_{\mathrm{a}}^*|, |\delta P_{\mathrm{b}}^*|, |\delta P_{\mathrm{c}}^*|\} = |\delta P_{\mathrm{b}}^*|$, then

$$\phi_0' = \begin{cases}-2\pi/3 & \delta P_{\mathrm{b}}^* \geq 0\\ \pi/3 & \delta P_{\mathrm{b}}^* < 0\end{cases} \tag{22}$$

If $\max\{|\delta P_{\mathrm{a}}^*|, |\delta P_{\mathrm{b}}^*|, |\delta P_{\mathrm{c}}^*|\} = |\delta P_{\mathrm{c}}^*|$, then

$$\phi_0' = \begin{cases}2\pi/3 & \delta P_{\mathrm{c}}^* \geq 0\\ -\pi/3 & \delta P_{\mathrm{c}}^* < 0\end{cases} \tag{23}$$

The selection principles of the phase angle for injection of zero-sequence voltage are then discussed.

In order to make the maximum utilization of negative-sequence current injection, the phase angle φ_n' is calculated using (24)–(26) to achieve the maximum active power flow with the same amplitude of δI_n.

3) Calculation of amplitudes: With the phase angle ϕ_0' and φ_n' calculated earlier, the amplitude of zero-sequence voltage and negative-sequence current, δU_0 and δI_n, can be expressed as (27) by substituting (18)–(20) and (24)–(26) into (17).

If $\max\{|\delta P_{\mathrm{a}}^*|, |\delta P_{\mathrm{b}}^*|, |\delta P_{\mathrm{c}}^*|\} = |\delta P_{\mathrm{a}}^*|$, then

$$\varphi_n' = \begin{cases}0 & \delta P_{\mathrm{a}}^* \geq 0\\ \pi & \delta P_{\mathrm{a}}^* < 0\end{cases} \tag{24}$$

If $\max\{|\delta P_{\mathrm{a}}^*|, |\delta P_{\mathrm{b}}^*|, |\delta P_{\mathrm{c}}^*|\} = |\delta P_{\mathrm{b}}^*|$, then

$$\varphi_n' = \begin{cases}2\pi/3 & \delta P_{\mathrm{b}}^* \geq 0\\ -\pi/3 & \delta P_{\mathrm{b}}^* < 0\end{cases} \tag{25}$$

If $\max\{|\delta P_{\mathrm{a}}^*|, |\delta P_{\mathrm{b}}^*|, |\delta P_{\mathrm{c}}^*|\} = |\delta P_{\mathrm{c}}^*|$, then

$$\varphi_n' = \begin{cases}-2\pi/3 & \delta P_c^* \geq 0\\ \pi/3 & \delta P_c^* < 0\end{cases} \tag{26}$$

$$\begin{cases}\delta U_0 = \dfrac{H_1\delta P_{\mathrm{b}}^* - H_2\delta P_{\mathrm{a}}^*}{H_1H_3 - H_2H_4}\\ \delta I_n = \dfrac{H_4\delta P_{\mathrm{b}}^* - H_3\delta P_{\mathrm{a}}^*}{H_2H_4 - H_1H_3}\end{cases} \tag{27}$$

where δP_{a}^* and δP_{b}^* are active power instructions of phase A and phase B. H_1, H_2, H_3 and H_4 are shown in (28).

$$\begin{cases} H_1 = U_p \cos\varphi'_n + U_0 \cos(\phi_0 - \varphi'_n) \\ H_2 = U_p \cos(\varphi'_n - 2\pi/3) + U_0 \cos(\phi_0 - \varphi'_n - 2\pi/3) \\ H_3 = I_p \cos(\phi'_0 - \varphi_p + 2\pi/3) + I_0 \cos(\phi'_0 - \varphi_n - 2\pi/3) \\ H_4 = I_p \cos(\phi'_0 - \varphi_p) + I_0 \cos(\phi'_0 - \varphi_n) \end{cases} \tag{28}$$

4) Transformation into *dq* frame: With the calculated phase angle and amplitude of extra zero-sequence voltage and negative-sequence current, the injection components are expressed in (29). In order to establish a unified frame, the extra zero-sequence voltage and negative-sequence current injection are then transformed into *dq* frame as (30) by substituting (18)–(29) into (9).

$$\begin{cases} \delta u_0 = \delta U_0 \cos(\omega t + \phi'_0) \\ \delta i_n = \delta I_n \cos(\omega t + \varphi'_n) \end{cases} \tag{29}$$

$$\begin{cases} \delta u_0 = \delta U_0 \cos(\omega t + \phi'_0) \\ \delta i_d = \delta I_n(\cos(\omega t + \varphi'_n)\sin\omega t + \sin(\omega t + \varphi'_n)\cos\omega t) \\ \delta i_q = \delta I_n(\sin(\omega t + \varphi'_n)\sin\omega t - \cos(\omega t + \varphi'_n)\cos\omega t) \end{cases} \tag{30}$$

4.4 Individual voltage balancing control

Individual voltage balancing control focuses on regulating the individual voltage of each capacitor in the same phase cluster and the control target is to keep U_{dckj} equal to the average value in the same phase cluster. This paper adopts duty cycle adjustment method to realize the individual voltage balancing control. Figure 5 shows the block diagram of individual voltage balancing control. Where U^*_{dckj} ($U^*_{dckj} = U_{dck}/N$) is the average voltage of the capacitor in each cluster. v^*_{ia}, v^*_{ib} and v^*_{ic} are the output references of the three-phase current controllers. Among them, k = a,b,c and j = 1, 2, …, N.

Since the capacitor voltage is determined by the active power flowing into each module, the capacitor voltage can be regulated by adjusting the power of each module. The power flow of each module can be regulated according to the direction of the output current. The output of the controllers v^*_{dckj} is added directly to the output of the current controllers. The final output is sent to the PWM unit. The sign function is shown as follows:

$$sign = \begin{cases} -1 & i_k > 0 \\ 1 & i_k < 0 \end{cases} \tag{25}$$

1) *Case 1* ($i_k > 0$): When the capacitor voltage U_{dckj} is smaller than the reference U^*_{dckj}, the value of sign function will be −1, v^*_{dckj} will be negative and the duty circle of this module will decrease. As a result, this module will emit less power to the grid and U_{dckj} will increase. On the contrary, when the capacitor voltage U_{dckj} is higher than the reference U^*_{dckj}, v^*_{dckj} will be positive and the duty circle of this module will increase. As a result, this module will emit more power to the grid and U_{dckj} will drop.

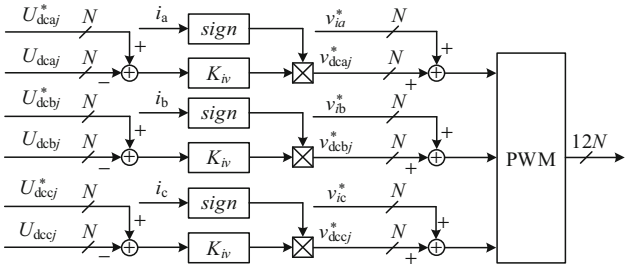

Fig. 5 Block diagram of individual voltage balancing control

2) *Case 2* ($i_k < 0$): When the capacitor voltage U_{dckj} is smaller than the reference U^*_{dckj}, the value of sign function will be 1, v^*_{dckj} will be positive and the duty circle of this module will increase. As a result, this module will absorb more power from the grid and U_{dckj} will increase. On the contrary, when the capacitor voltage U_{dckj} is higher than the reference U^*_{dckj}, v^*_{dckj} will be negative and the duty circle of this module will decrease. As a result, this module will absorb less power from the grid and U_{dckj} will drop.

The main idea of duty cycle adjustment is to make the module absorb more power or emit less power when $U_{dckj} < U^*_{dckj}$, and absorb less power or emit more power when $U_{dckj} > U^*_{dckj}$. Individual voltage balancing is thus realized.

5 Simulation and experimental results

5.1 Simulation results

The simulation model of three-phase STATCOM with star connection is established according to Fig. 1. To verify the performance of the proposed control strategy, several simulations have been carried out in MATLAB simulation environment. The studied system parameters are shown in Table 1.

Figure 6 illustrates the dynamic responses of cascaded STATCOM operation from 15 kvar capacitive reactive power to 15 kvar inductive reactive power. Figure 6a shows three-phase clustered voltages and Fig. 6b shows the four individual capacitor voltages of phase A. Figure 6c depicts the grid voltage of phase A and three-phase output currents of STATCOM and Fig. 6d shows the grid voltage of phase A and three-phase grid currents. The voltage scale

Table 1 Simulation parameters

Parameters	Symbol	Value
Line to line voltage	u_g	380 V
Grid frequency	f_g	50 Hz
Rated reactive power	Q	15 kvar
Cell numbers per phase	N	4
AC filter inductor	L	10 mH
DC capacitor	C	3000 μF
DC voltage	U_{dc}	350 V
Switch frequency	f_s	1.25 kHz

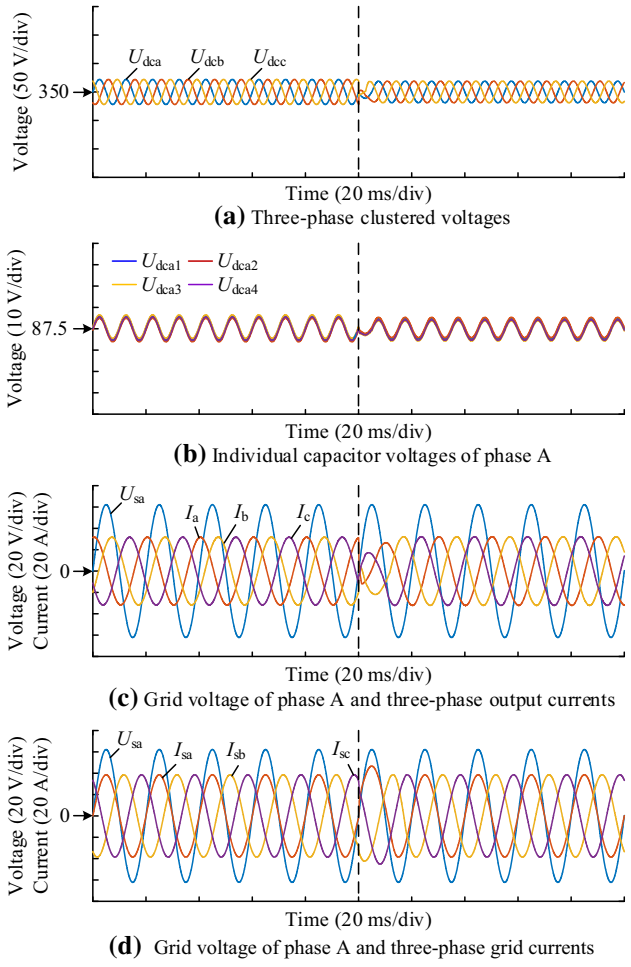

Fig. 6 Dynamic responses of STATCOM operation under different kinds of reactive power generation

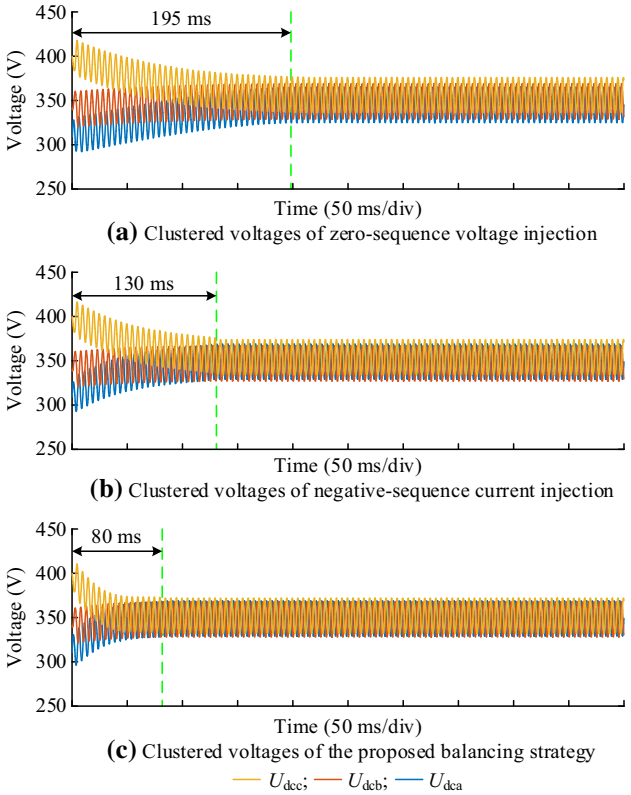

Fig. 7 Dynamic responses of clustered voltages with different balancing strategies

of phase A in Fig. 6c and d is 1:5 to provide a clearer view of the phase angle of the currents. As is shown in Fig. 6, the three-phase clustered voltages and individual voltages are well balanced in operation of both maximum capacitive and inductive reactive power generation.

To verify the superiority of the proposed clustered voltage balancing strategy, additional simulations are conducted with three voltage balancing strategies (zero-sequence voltage injection, negative-sequence current injection and proposed clustered voltage balancing strategy). To derive an unbalanced clustered voltage, the initial voltages of the three clusters are 310 V, 340 V and 400 V individually. The STATCOM is set to generate capacitive reactive current of 20 A. Figure 7 shows the dynamic responses for the three voltage balancing strategies and Fig. 8 presents the negative-sequence current instructions of the negative-sequence current injection method and the proposed balancing method. As is shown in Fig. 7a, the zero-sequence voltage injection method needs about 195 ms to balance the voltages of the three clusters and has a relatively slow response and low efficiency in clustered voltage balancing. Figure 7b reflects that the negative-sequence current injection method needs about 130 ms to balance the voltages of the three clusters and is more effective. Nevertheless, the balancing response is not as

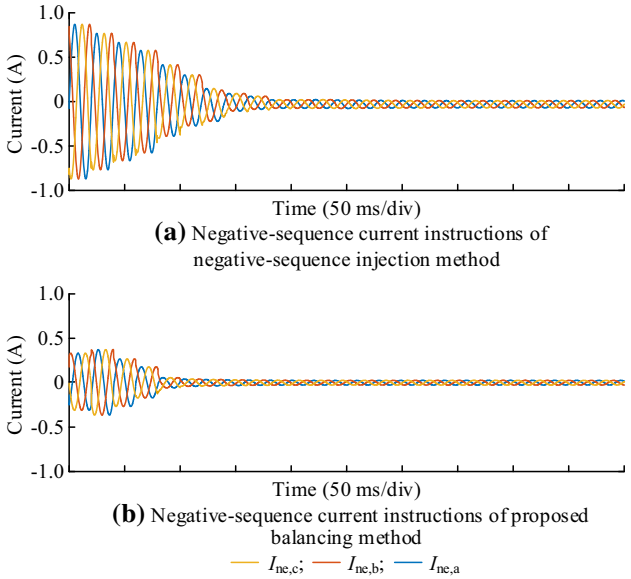

Fig. 8 Negative-sequence current instructions with different balancing strategies

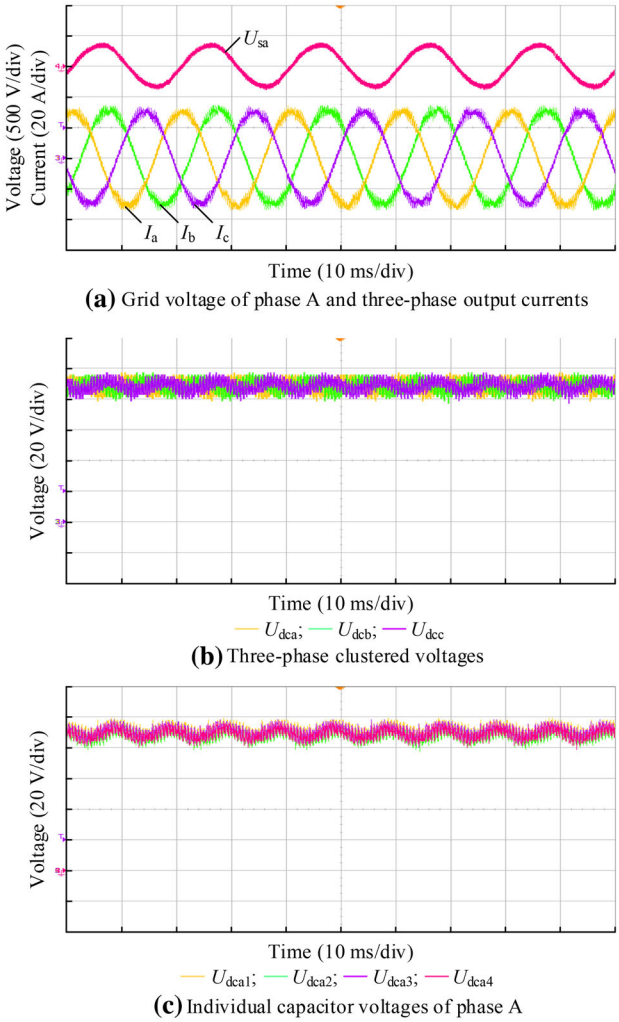

Fig. 9 Steady waveforms under operation of 15 kvar capacitive reactive power

fast as that of the proposed strategy. Figure 7c shows that the proposed control strategy with injections of zero-sequence voltage and negative-sequence current needs about 80 ms to balance the voltages of the three clusters and has a faster response than the other two balancing strategies. As shown in Fig. 8, the proposed balancing method has lower negative-sequence current instructions than the negative-sequence current injection method.

5.2 Experimental results

To verify the effectiveness of the proposed control strategy, experiments have been conducted. The system parameters are the same as the simulation parameters shown in Table 1. In this paper, unless otherwise mentioned, the attenuation ratio of the voltage and current probe is 1:100. The minimum voltage unit and the minimum time unit are shown on the top of each figure.

The steady waveforms under operation of 15 kvar capacitive reactive power and 15 kvar inductive reactive power are shown individually in Figs. 9 and 10.

Figure 9a shows the grid voltage of phase A and three-phase output currents under operation of 15 kvar capacitive reactive power. To verify the effectiveness of the proposed clustered voltage balancing strategy, DC voltage waveforms of the first module in each phase are collected. Considering that the individual voltage balancing control can balance the voltage of each module in the same phase, the value of the clustered voltage will be four times ($N = 4$) that of the individual voltage. Figure 9b shows the voltages of the first module in three phases and Fig. 9c shows the voltages of the four modules in phase A.

Figure 10a shows the grid voltage of phase A and three-phase output currents under operation of 15 kvar inductive reactive power. To verify the effectiveness of the proposed clustered voltage balancing strategy, DC voltage waveforms of the first module in each phase are collected. Figure 10b shows the voltages of the first module in three phases and Fig. 10c shows the voltages of the four modules

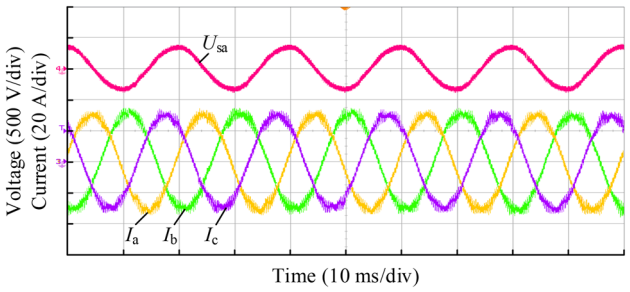

(a) Grid voltage of phase A and three-phase output currents

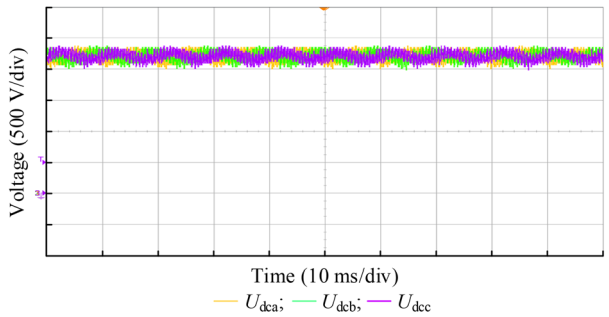

(b) Three-phase clustered voltages

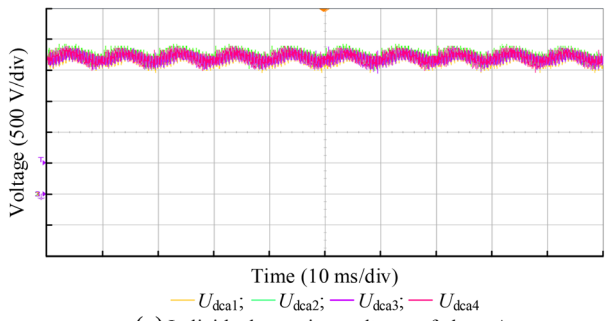

(c) Individual capacitor voltages of phase A

Fig. 10 Steady waveforms under operation of 15 kvar inductive reactive power

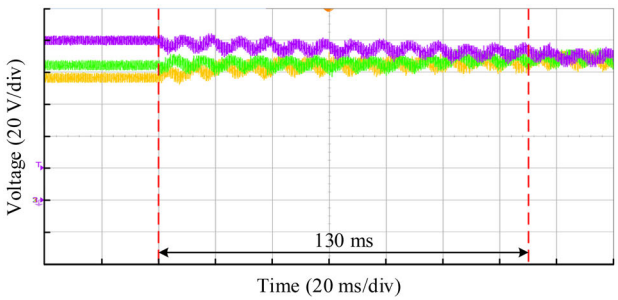

(a) Clustered voltages of zero-sequence voltage injection

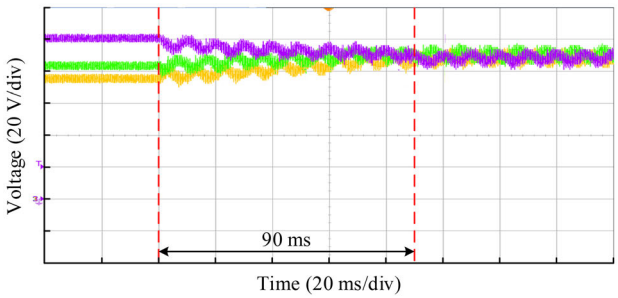

(b) Clustered voltages of negative-sequence current injection

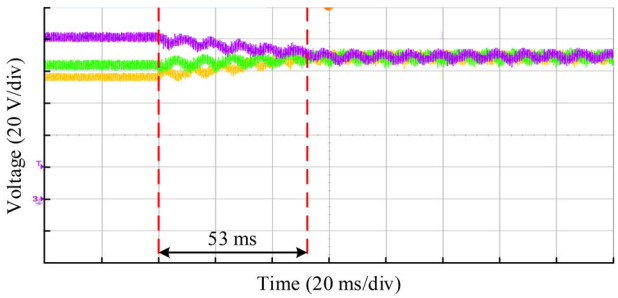

(c) Clustered voltages of the proposed balancing strategy

U_{dca}; U_{dcb}; U_{dcc}

Fig. 11 Experimental waveforms of clustered voltages with different balancing strategies

in phase A. As is shown in Figs. 9 and 10, the clustered voltages and individual voltages are well balanced. The effectiveness of the proposed control strategy is thus verified.

Figure 11 demonstrates the experimental voltage waveforms of the first module in each phase under different balancing strategies. The initial voltages of the three clusters are 310 V, 340 V and 400 V individually, and the corresponding voltages of the first modules are 77.5 V, 85 V and 100 V. The STATCOM is set to generate capacitive reactive current of 20 A. The dynamic balancing period of zero-sequence voltage injection method, negative-sequence current injection method and the proposed voltage balancing method are approximately 130 ms, 90 ms and 53 ms, respectively. The experimental results verify the superiority of the proposed voltage balancing strategy.

6 Conclusion

In this paper, the reasons behind the occurrence of unbalanced clustered voltage are analyzed first. This phenomenon is theoretically proved to be caused mainly by the compensation of unbalanced reactive power, detection or control errors, and voltage drift of STATCOM neutral point. Subsequently, this paper proposes a novel control strategy which injects negative-sequence current and zero-sequence voltage simultaneously. The simulation results prove that the proposed control strategy has a faster dynamic response. The proposed control strategy can also lower the extent of current asymmetry by reducing the negative-sequence current injection. The experimental results show the effectiveness and superiority of the proposed control strategy in clustered voltage balancing.

References

[1] Lu D, Wang J, Yao J et al (2017) Clustered voltage balancing mechanism and its control strategy for star-connected cascaded h-bridge statcom. IEEE Trans Ind Electron 64(10):7623–7633
[2] Reddy CL, Kumar PS, Sushama M et al (2015) A five level cascaded H-bridge multilevel STATCOM. In: Proceedings of IEEE Asia Pacific conference on postgraduate research in microelectronics and electronics, Hyderabad, India, 27–29 November 2015, 6 pp
[3] Hu Y, Ren J, Wang J et al (2011) Analysis of voltage unbalance phenomenon and causes in cluster DC link of cascaded H-bridge STATCOM. Automat Electr Power Syst 35(21):96–100
[4] Akagi H, Inoue S, Yoshii T (2007) Control and performance of a transformerless cascade PWM STATCOM with star configuration. IEEE Trans Ind Appl 43(4):1041–1049
[5] Zhao L, Shi YJ, Duan SX et al (2009) The research of DC capacitance voltages balancing strategy based on cascade STATCOM using individual phase instantaneous current tracking. In: Proceedings of IEEE international power electronics and motion control conference, Wuhan, China, 17–20 May 2009, 5 pp
[6] Xu R, Yu Y, Yang R et al (2014) A novel control method for individual DC voltage balancing in H-bridge cascaded STATCOM. In: Proceedings of international power electronics conference, Hiroshima, Japan, 18–21 May 2014, 5 pp
[7] Neyshabouri Y, Iman-Eini H, Farhangi S (2013) Control of a transformer-less cascaded H-bridge based STATCOM using low-frequency selective harmonic elimination technique. In: Proceedings of international conference on environment and electrical engineering, Wroclaw, Poland, 5–8 May 2013, 6 pp
[8] Neyshabouri Y, Iman-Eini H, Miranbeigi M (2015) State feedback control strategy and voltage balancing scheme for a transformer-less Stati synchronous compensator based on cascaded H-bridge converter. Power Electron IET 8(6):906–917
[9] Barrena JA, Marroyo L, Vidal MAR et al (2008) Individual voltage balancing strategy for PWM cascaded H-bridge converter-based STATCOM. IEEE Trans Ind Electron 55(1):21–29
[10] Marzoughi A, Neyshabouri Y, Imaneini H (2014) Control scheme for cascaded H-bridge converter-based distribution network static compensator. Power Electron IET 7(11):2837–2845
[11] Lei E, Yin X, Zhang Z et al (2018) An improved transformer winding tap injection DSTATCOM topology for medium-voltage reactive power compensation. IEEE Trans Power Electron 33(3):2113–2126
[12] Sun Y, Zhao J, Ji Z et al (2013) An improved DC capacitor voltage balancing strategy for PWM cascaded H-bridge converter-based STATCOM. In: Proceedings of international conference on power electronics and drive systems, Kitakyushu, Japan, 22–25 April 2013, 6 pp
[13] Guo S, Liu D (2010) Voltage oriented based control strategy for cascaded PWM STATCOM. In: Proceedings of Asia-Pacific power and energy engineering conference, Chengdu, China, 28–31 March 2010, 4 pp
[14] Townsend CD, Cox SM, Watson AJ et al (2012) Voltage balancing characteristics for a cascaded H-bridge multi-level STATCOM employing space vector modulation. Novi Sad, Serbia, 4–6 September 2012, 7 pp
[15] Su Z, Zeng G, Zhang J et al (2012) The DC capacitors' voltage balancing strategy for cascaded H-bridge converter based STATCOM. In: Proceedings of IEEE international power electronics and motion control conference, Harbin, China, 2–5 June 2012, 4 pp
[16] Behrouzian E, Bongiorno M, Teodorescu R et al (2015) Individual capacitor voltage balancing in H-bridge cascaded multilevel STATCOM at zero current operating mode. In: Proceedings of European conference on power electronics and applications, Geneva, Switzerland, 8–10 September 2015, 10 pp
[17] Maharjan L, Inoue S, Akagi H (2008) A transformerless energy storage system based on a cascade multilevel PWM converter with star configuration. IEEE Trans Ind Appl 44(5):1621–1630
[18] Maharjan L, Yamagishi T, Akagi H (2012) Active-power control of individual converter cells for a battery energy storage system based on a multilevel cascade PWM converter. IEEE Trans Power Electron 27(3):1099–1107
[19] Hatano N, Ise T (2010) Control scheme of cascaded H-bridge STATCOM using zero-sequence voltage and negative-sequence current. IEEE Trans Power Deliv 25(2):543–550
[20] Chen HC, Cheng PT (2015) Improved DC voltage utilization for the star-connected cascaded H-bridges converter under unbalanced voltage sags. In: Proceedings of 9th international conference on power electronics and ECCE Asia, Seoul, South Korea, 1–5 June 2015, 8 pp
[21] Chen HC, Cheng PT (2017) A DC bus voltage balancing technique for the cascaded H-bridge STATCOM with improved reliability under grid faults. IEEE Trans Ind Appl 53(2):1263–1270
[22] Han C, Huang AQ, Liu Y et al (2007) A generalized control strategy of per-phase DC voltage balancing for cascaded multilevel converter based STATCOM. In: Proceedings of IEEE power electronics specialists conference, Orlando, USA, 17–21 June 2007, 7 pp
[23] Lee C, Chen H, Wang C et al (2014) A flexible DC voltage balancing control based on the power flow management for star-connected cascaded H-bridge converter. In: Proceedings of IEEE energy conversion congress and exposition, Pittsburgh, USA, 14–18 September 2014, 8 pp

Yu JIN received B.S. degree from School of Electrical Engineering and Automation, Harbin Institute of Technology, Harbin, China. He is currently working as a Ph.D. student in School of Electrical Engineering and Automation, Harbin Institute of Technology. His research interests include control method and applications of Half/Full bridge modular multilevel converter including STATCOM, motor driver, MMC-based energy storage system.

Jianze WANG received the B.E., M.E., and Ph.D. degrees in Electrical Engineering from the Harbin Institute of Technology, Harbin, China, in 1993, 1996, and 1999, respectively. He joined the Harbin Institute of Technology, in 1999, and is currently a Research Professor. From July 2003 to December 2003, he was a Visiting Scholar with the Hong Kong Polytechnic University, Hong Kong, China. His current research interests include power electronics, multilevel converters, and digital-signal-processor-based power quality control systems.

Yiqi LIU received the B.S. degree in Electrical Engineering from Northeast Agriculture University, Harbin, China, in 2009, the M.S.

degree in Electrical Engineering from the Tianjin University of Technology, Tianjin, China, in 2012, and the Ph.D. degree in electrical engineering from the Harbin Institute of Technology, Harbin, China, in 2016. He joined Northeast Forestry University, Harbin, China, in 2016, where he is currently an Associate Professor. His current research interests include power electronics for renewable energy sources, multilevel converters, high-voltage direct-current technology, and microgrid clusters.

Xiangyu SAI received B.S. degree from School of Electrical Engineering and Automation, Harbin Institute of Technology, Harbin. He is a M.S. candidate of Electrical Engineering and Automation at Harbin Institute of Technology. His research interests include the control strategy and applications of active power filters, battery's SOC in large-capacity energy storage system.

Yanchao JI received the B.E., and M.E. degrees in Electrical Engineering from Northeast Electric Power University, Jilin, China, in 1983 and 1989, respectively, and the Ph.D. degree in Electrical Engineering from the North China Electric Power University, Beijing, China, in 1993. He joined the Department of Electrical Engineering, Harbin Institute of Technology, Harbin, China in 1993. From 1995 to 1996, he was an Associate Professor with the Department of Electrical Engineering, Harbin Institute of Technology, where he is currently a Professor. His current research interests include pulse width modulation technique, power converter, and flexible AC transmission systems devices.

STATE GRID
STATE GRID ELECTRIC POWER RESEARCH INSTITUTE